ACS APPLIED ELECTRONIC MATERIALS

pubs.acs.org/acsaelm Article

Full Activation of Dopants by Carbon-free Self-Assembled Molecular Monolayer Doping

Kai Li, Jie-Yin Zhang, Shannan Chang, Hao Wei, Jian-Jun Zhang, and Yaping Dan*

Cite This: ACS Appl. Electron. Mater. 2021, 3, 3346−3351 Read Online

ACCESS | Metrics & More | Article Recommendations | Supporting Information

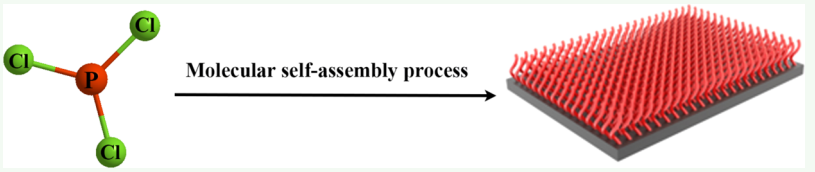

ABSTRACT: Self-assembled molecular monolayer doping may find important applications in doping FinFET and nanowire transistors due to its nature of being conformal, nondestructive, and self-limiting. However, carbon contamination from the dopant carrier molecules is often introduced into silicon, which will affect the device performance. Herein, we use carbon-free phosphorus chloride (PCl_3) molecules as dopant carrier molecules to avoid the introduction of carbon contamination. The Hall effect measurements and secondary ion mass spectrometry show that the dopant activation rate is close to full activation even for samples with a low doping concentration.

KEYWORDS: *monolayer doping, carbon free, molecular self-assembly, Hall effect, electrical activation*

INTRODUCTION

The successful development of integrated circuits (IC) is mainly driven by the constant size downscaling of complementary metal-oxide-semiconductor (CMOS) field effect transistors (FETs).[1,2] In the past decade, the IC industry has come across a point where the short channel effect is playing a critical role in the operating principle of modern ultra-scaled field effect transistors that will eventually result in the failure of CMOS transistors if not properly addressed.[3] Forming an ultra-shallow junction in the source and drain region of the transistors is an effective approach to mitigate the short channel effect.[4] In 2008, Javey et al. demonstrated that self-assembled molecular monolayer (SAMM) doping can form ultra-shallow doping in silicon with controllable doping concentration.[5] In this SAMM doping technique, dopant carrying molecules are first covalently grafted onto the semiconductor surfaces, forming a monolayer of molecules. The dopants are then driven into the semiconductor substrate by rapid or spike thermal annealing. It is well known that doping by ion implantation suffers from lattice damages and unsuitability for three-dimensional (3D) semiconductor structures such as FinFETs[6−8] as well as the difficulty to form ultra-shallow doping junctions. In contrast, the SAMM doping is a mild doping technique that causes no lattice damages. The self-assembly nature of the SAMM doping will form a uniform and conformal coverage of semiconductor surfaces and therefore is compatible with 3D or complex structure doping.[9−11]

However, we recently found that carbon impurities of the dopant carrying molecules were driven into the silicon lattice along with the dopant atoms, partially or seriously deactivate the electrical activity of phosphorus dopant atoms depending on the doping concentrations,[9,12,13] although carbon impurities in p-type Si form minority traps and have a limited impact on acceptor-type dopants.[14] It is thus important to develop a carbon-free SAMM doping technology, which has been explored in recent years. To avoid the introduction of carbon impurities into the substrate, Longo et al.[15,16] and Zhi et al.[17] used low temperature pyrolysis to break the P−C bond at 500 °C before high temperature annealing treatment and then released the alkane chain in the octadecylphoshponic acid (ODPA) molecule. To improve the activation rate of phosphorus, Gao et al.[18] extending the thermal annealing time to separate interstitial carbon (C_i) from the phosphorus dopants by taking the advantage of the difference in the diffusion coefficient of carbon and phosphorus. van Drunen et al.[19] formed an ultra-thin SiO_2 layer on the silicon surface through the pre-treatment process of RCA to prevent the carbon diffusion into the silicon. This group also used phosphorus pentoxide as the dopant source that does not contain carbon atoms. However, phosphorus pentoxide needs to be grafted on the surface of silicon oxide to achieve semiconductor doping. Although carbon pollution can be

Received: March 22, 2021
Accepted: July 15, 2021
Published: August 2, 2021

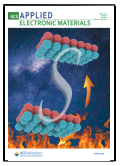

https://doi.org/10.1021/acsaelm.1c00276
ACS Appl. Electron. Mater. 2021, 3, 3346−3351

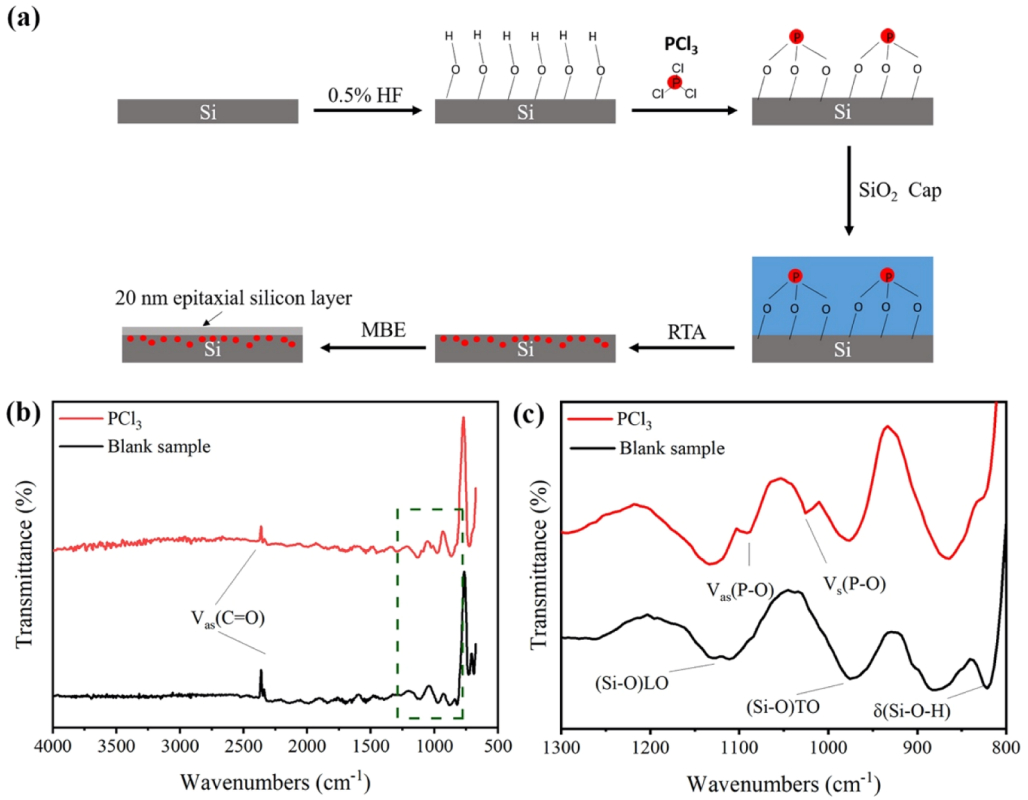

Figure 1. (a) Stepwise surface modification on Si(100) surfaces using phosphorus trichloride molecules and infrared transmission spectra taken from (b) PCl_3 modified sample and blank sample. Note that the blank silicon wafer went through the same process except the reaction with PCl_3. The peaks labeled as $V_{as}(C{=}O)$ are related to the CO_2 molecules in air. (c) Zoom-in IR spectra of the characteristic infrared peaks of P−O bonds in the dashed window in (b).

avoided, the oxide layer is a barrier for the efficient incorporation of phosphorus in the monolayer into the underlying devices, resulting in the uncertainty in controlling the dopant concentration and profile. Ye et al.[20] synthesized an organic carborane with a small carbon-boron ratio as a doping molecule, thereby reducing carbon pollution while ensuring high doping. However, these methods cannot completely prevent the formation of carbon-related defect states during the SAMM doping process.

In this work, we used phosphorus trichloride (PCl_3) as the dopant-carrying molecules to avoid the introduction of carbon impurities. PCl_3 molecules were grafted on OH-terminated Si surfaces, forming $(SiO)_3P$-terminated surfaces. P dopants were driven into silicon by rapid thermal annealing. To avoid the surface effect and increase the activation rate of phosphorus dopants in silicon, a 20 nm thick crystalline was epitaxially grown on the silicon surface after the sample was properly cleaned. Hall effect measurements and secondary ion mass spectrometry (SIMS) profiling show that the electrical activation rate of phosphorus dopants is higher than 90% even at low doping concentration.

RESULTS AND DISCUSSION

Figure 1a shows the self-assembly process of phosphorus trichloride (PCl_3) on the silicon surface. Briefly, intrinsic silicon-on-insulator (SOI) substrates were thoroughly cleaned before immersed in a 0.5% HF solution for 5 s to remove the natural oxide layer. At the same time, Si−O−H bonds formed on the silicon surfaces,[11] although Si−H bonds often form on the Si surfaces after treated with a high concentration of HF solution. The sample was then quickly transferred to a reaction flask containing PCl_3 molecules. The PCl_3 molecules were grafted on the Si surfaces with the assistance of triethylamine as the catalyst. After a period of reaction time in the flask, the samples were first cleaned and then covered with a 200 nm thick SiO_2 layer using magnetron sputtering (Denton vuucm, WF1DMSP01). Finally, the standard rapid thermal annealing (RTA) process was applied to anneal the samples at 1050 °C for 30 s to drive the dopants into the silicon substrate. After the RTA process, a 20 nm-thick crystalline silicon was epitaxially grown on top of the doped sample after the SiO_2 coating was removed with 2.5% HF solution and surface cleaning in ultra-high vacuum. Samples with different doping concentrations were obtained in the same approach by changing the reaction time of the reactants. Two sets of samples were made with one for 6 h reaction and the other for 1 h reaction. The samples were labeled as PCl_3-h and PCl_3-l for the relatively high and low doping concentration, respectively.

To check whether PCl_3 molecules were successfully grafted on silicon surfaces, we first characterized the sample surfaces using Fourier transform infrared (FTIR) spectroscopy. Figure 1b shows the FTIR spectra of the samples grafted with PCl_3 (red) and the blank Si sample (black). No stretching vibrations of CH_2 and CH_3 (around 2800−3000 cm^{-1}) and aliphatic hydrocarbons were detected in both samples, indicating that no carbon contaminants were introduced during the self-assembly of PCl_3 molecules. Indeed, weak stretching and asymmetric stretching vibration modes of P−O bonds were detectable at 1091 and 1024 cm^{-1}, respectively (Figure 1b). It shows that PCl_3 molecules were successfully self-assembled on

https://doi.org/10.1021/acsaelm.1c00276
ACS Appl. Electron. Mater. 2021, 3, 3346−3351

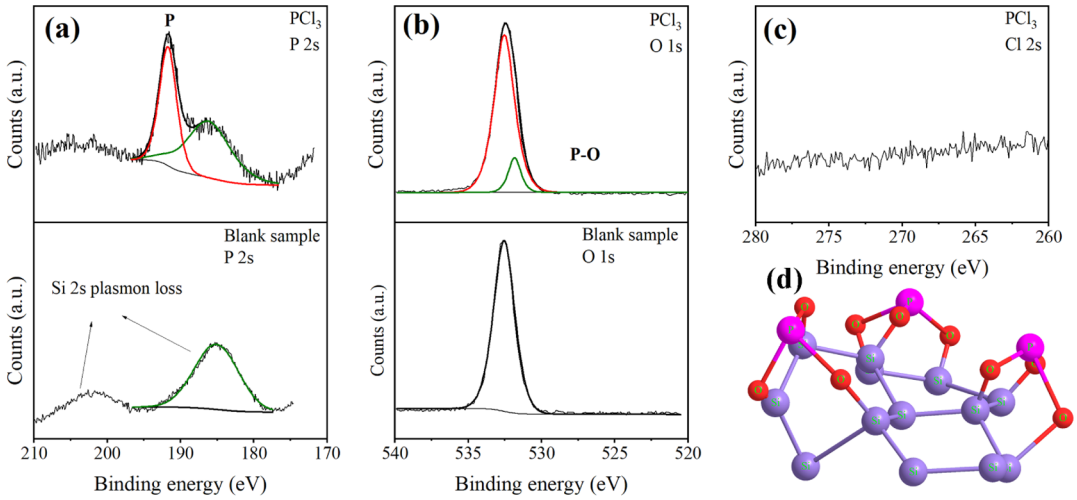

Figure 2. XPS spectra of blank and modified silicon samples. (a) P 2s spectrum of silicon modified with PCl_3 and blank sample. (b) O 1s spectrum of silicon modified with PCl_3 and blank sample. (c) Cl 2s spectrum of silicon modified with PCl_3. (d) Surface molecular structure of silicon modified with PCl_3.

the silicon surface. In addition, stretching vibrations (856−820 cm^{-1}) belonging to Si−O−H are also visible, which is caused by the exposure of the sample to the atmosphere during preparation or characterization. The unbonded Si dangling bonds would be oxidized by intrusive oxygen, forming sub-stoichiometric SiO_x (x <2).

X-ray photoelectron spectroscopy (XPS) was also employed to characterize the Si surfaces that were grafted with PCl_3 (see Figure S1 in Supporting Information for the full XPS spectrum). A strong peak of the P 2s at 191.7 eV is clearly visible (top panel in Figure 2a) on top of two Si 2s plasma broad bumps on the blank silicon sample (bottom panel in Figure 2a). This indicates that a high concentration of PCl_3 molecules has successfully grafted on the silicon surfaces. PCl_3 molecules bind with silicon likely in a form of Si−O−P because the O 1s peak of the PCl_3 grafted sample can be decomposed into a main peak at 532.5 eV (1.7 eV in FWHM) and a small peak 531.8 eV (1.0 eV in FWHM). The main peak at 532.5 eV is the typical characteristics of O 1s in the form of SiO_x and SiOH for blank silicon. The small peak at 531.8 eV is attributed to P−O bonds, indicating that the PCl_3 molecules are immobilized onto the silicon surfaces via the P−O bonds. However, since the peak at 531.8 eV is decomposed from the main peak and its magnitude is relatively weak, we cannot exclude the possibility that $P(OSi)_3$, $P(OSi)_2OH$, and $POSi(OH)_2$ may coexist. Nevertheless, the characteristic peak of the binding energy of Cl does not appear on the surfaces of the PCl_3 modified silicon surfaces. This observation shows that Cl ions of PCl_3 are completely removed during the grafting process via the possible chemical reaction 1.[21] The atomic force microscope (AFM) image of the PCl_3 modified sample is shown in Supporting Information, Figure S2. It can be seen from the figure that the surface of the sample after the reaction is very flat and there is no agglomeration, which indicates that the molecules were uniformly grafted on the silicon surface, but less likely a monolayer based on the secondary ion mass spectrometry (SIMS) shown later.

$$PCl_3 + 3SiOH \rightarrow P(-O-Si)_3 + 3HCl \quad (1)$$

After PCl_3 molecules were grafted onto the silicon surfaces, the Si sample was then covered with a 200 nm-thick SiO_2 film by sputtering. Rapid thermal annealing (RTA) was applied to drive the dopants into the silicon substrate at 1050 °C for 30 s. After removal of the SiO_2 film followed by metallization, van der Pauw four-point measurements were applied to characterize the blank sample and PCl_3-doped Si samples. The sheet resistance is measured according to the structure, as shown in Figure S3. To tune the doping concentration, we controlled the reaction time for grafting PCl_3 onto silicon surfaces. The sample with a high doping concentration (labeled as PCl_3-h) is the one with a reaction time of 6 h. The one with the shorter reaction (1 h) has the lower doping concentration (labeled as PCl_3-l). The measured sheet resistance is shown in Table 1.

Table 1. Sheet Resistance, Carrier Concentration, and Activation Rate of the Blank Sample and Doped Sample via the SAMM Doping Technique

sample	blank	PCl_3-h	PCl3-l
R_s (KΩ/sq)	2754.49	3.08	10.44
carrier concentration (cm^{-2}) from Hall measurements		3.47×10^{12}	6.21×10^{11}
dopant concentration (cm^{-2}) from SIMS		3.69×10^{12}	6.89×10^{11}
dopant activation rate		94.0%	90.1%

The sheet resistance (R_s) of the blank sample is 2754.49 KΩ/sq, indicating that no significant contamination was introduced during this process. After doping, the sheet resistances of the samples are reduced by 2−3 orders of magnitude to 3.08 KΩ/sq for the medium-doped sample (PCl_3-h) and 10.44 KΩ/sq for the lightly doped sample (PCl_3-l). The $I-V$ curve of each sample is shown in Supporting Information, Figures S4−S6.

It was reported that interstitial carbon impurities can reduce the activation rate of phosphorus dopants by C_i-P_s pairs.[12,17,18] To estimate the dopant activation rate of our samples, we need first to find the electron concentration by Hall effect measurements and then probe the dopant distribution profile by secondary ion mass spectroscopy (SIMS). For the Hall effect measurement, we swept the magnetic field intensity from −1T to 1T at a given current. The Hall resistance is linear with the magnitude field intensity, as shown in Figure 3a. The Hall resistance is nonzero at zero

https://doi.org/10.1021/acsaelm.1c00276
ACS Appl. Electron. Mater. 2021, 3, 3346−3351

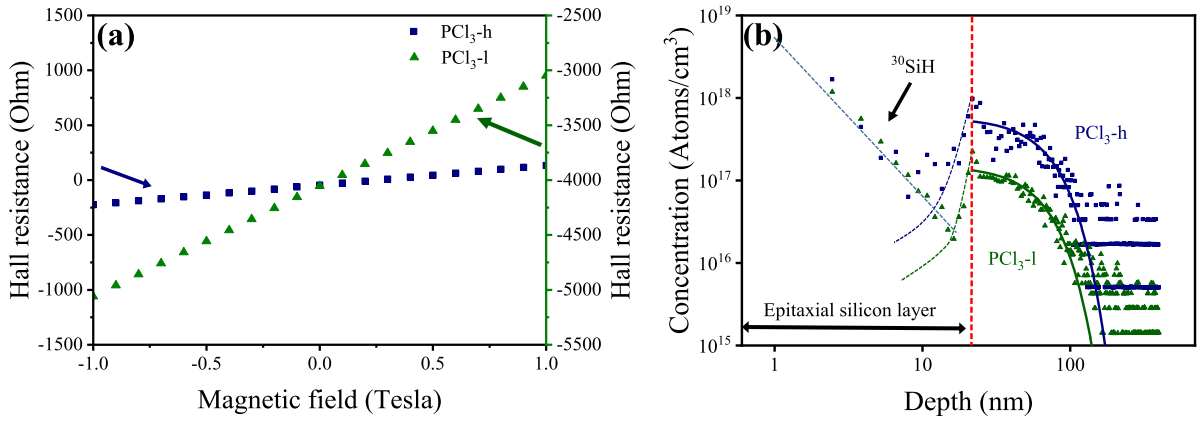

Figure 3. (a) Hall resistance of PCl_3-h and PCl_3-l versus magnetic field measured by Hall measurement at room temperature; (b) doping profile of PCl_3-h (blue dot) and PCl_3-l (green dot) measured by SIMS.

magnetic field intensity because the sample shape is not a perfect square (see Supporting Information Figure S3), resulting in the Hall bars asymmetrically placed across the applied current direction. The areal concentration of electrons can be calculated from the derivative of Hall resistance respective to magnetic field intensity following eq 2. The measured electron concentrations for the samples are summarized in Table 1.

$$N_e = -\frac{\Delta B}{e \times (\Delta V_H / I)} \quad (2)$$

e: unit charge; V_H: Hall voltage; I: source current; B: magnetic field; and N_e: free electron concentration per unit area.

The dopant distribution profile was probed by SIMS. It is well known that, however, SIMS is not accurate near the surfaces because the surfaces can be easily contaminated and the material interface is often not atomically sharp, making it difficult to estimate the dopant concentration. To address this issue, we epitaxially grew a 20 nm thick crystalline silicon on top of the PCl_3-doped Si samples after the sample surfaces were thoroughly cleaned. By doing so, SIMS will first profile the undoped surfaces before it reaches the critical interface between the epitaxial layer and the original substrate. The inaccuracy of phosphorus profile occurs only near the outer surfaces instead of the original surfaces before epitaxy. As shown in Figure 3b, the P profile has a peak located at 20 nm below the surface, which is the interface of the epitaxial layer and the original substrate surface. The P dopants diffuse well into the bulk following the limited source diffusion model, as shown in eq 3. Interestingly, the dopants also slightly diffuse into the epitaxial layer probably because the silicon layer was epitaxially grown at a relatively high temperature (450 °C). This diffusion causes the P concentration to decrease from the epitaxial interface to the surface but reach a minimal value at 10 nm below the surface and then surprisingly increases more by 1 order of magnitude at the surface. This surprising increase in P concentration is likely due to the "contamination" from $^{30}Si-H$ dimers which have the same mass with ^{31}P atoms.[22] From the SIMS profiles, we find the actual concentration of phosphorus in PCl_3-h and PCl_3-l is 3.69×10^{12} and 6.89×10^{11} cm^{-2}, respectively, as shown in Table 1.

$$N(x, t) = \left(\frac{N_d}{\sqrt{\pi D t}}\right) \exp\left[-\left(\frac{x}{2\sqrt{Dt}}\right)^2\right] \quad (3)$$

where N_d is the initial surface concentration (doping dose), x is the doping depth, t is the annealing time, and D is the diffusivity.

Based on the Hall measurements and SIMS results, we can calculate the electrical activation rate of dopants. The P activation rates of our PCl_3-doped samples are all over 90%. The sample with a higher doping concentration has a high dopant activation rate, which is consistent with our previous observations.[9,12] We also performed a long-time (24 h) surface modification to increase the doping concentration to 3.44×10^{14} cm^{-2}. The activation rate calculated from Hall effect measurements and SIMS profiling reaches 101%. The slightly higher than 100% is likely caused by the error in SIMS profiling. For comparison, we also repeated the experiments using diethyl vinylphosphonate (DVP) molecules. The resultant P concentration is 5.74×10^{12} cm^{-2} and the dopant activation rate is 78%, lower than our samples. These data are included in the Supporting Information from Figure S7–S10. The high activation rate of P dopants in our samples is in line with the fact that the dopant-carrying molecules are carbon-free, although some carbon contamination is still detectable at the interface of the epitaxial layer and the original wafer surface (Figure S11). Further analysis indicates that the carbon contamination likely comes from the sample exposure to the air.

CONCLUSIONS

In this work, we have investigated a carbon-free self-assembled molecular monolayer doping technique, in which PCl_3 molecules were used as the doping source. To reliably find the dopant activation rate, we employed Hall effect measurements to find the electron concentration after the monolayer doping and epitaxially grew 20 nm-thick single crystalline Si on top of the doped Si substrate for more reliable SIMS profiling. Because the molecule does not contain carbon contaminants, phosphorus dopants introduced into silicon by PCl_3 are close to full ionization.

METHODS

Materials. FZ Intrinsic Si(100) wafers (resistivity: ≥10 kΩ·cm; thickness: 500 ± 10 μm, top silicon 10 μm) were purchased from Suzhou Resemi Semiconductor Company. The acetone, ethanol, and methanol used for silicon surface cleaning and sample preparation are CMOS electronic grades, which were purchased from Sinopharm Chemical Reagent Company and Sigma-Aldrich (Shanghai) Com-

https://doi.org/10.1021/acsaelm.1c00276
ACS Appl. Electron. Mater. 2021, 3, 3346−3351

pany, respectively. Other reagents were analytical reagents without special instructions. Toluene (98%) was purchased from Sinopharm Chemical Reagent Co., Ltd. Phosphorus trichloride (PCl_3, 99%) was purchased from Innochem. Triethylamine (99.5%, GC) was purchased from Aladdin. Hydrofluoric acid (HF, 48%, CMOS electronic grade) comes from Sigma-Aldrich.

Pre-processing of Silicon Wafer. Silicon wafers were cleaved into 1.2 cm by 1.2 cm pieces, and the local top silicon from the edge 1 mm was etched away, leaving only the top silicon area of 1 cm by 1 cm. Then, the silicon samples were cleaned with isopropanol, acetone, ethanol of CMOS grade, and deionized water in a sonication bath for 3 min. Finally, the silicon wafers were dried with N_2.

Self-Assembly of PCl_3 on the Silicon Surface. The pre-treated silicon wafers were etched in 0.5% HF solution for 5 s to form the OH-terminated surface. The silicon wafers were quickly washed with deionized water and dried with N_2 and then transferred to a glovebox to prepare for the reaction. 10 mL of toluene and 2.4 mL of triethylamine were added into the reaction bottle, and then, the silicon wafers were put into the solution. Then, 0.5 mL of phosphorus trichloride was dropped into the reaction flask. The whole reaction took place at 70 °C for 1 and 6 h. After the reaction was completed, they were washed with acetone, ethanol, and deionized water in a sonication bath for 3 min. The ultrasound process was carried out to remove the chemical molecules on the adsorption surface. Finally, the cleaned silicon wafers were dried with N_2.

Silica Deposition and Thermal Annealing. The SiO_2 coating layer on silicon was a method of sputtering through a multi-target magnetron sputtering system. The thickness of SiO_2 was 200 nm. Then, RTA treatment was carried out at 1050 °C for 30 s to diffuse phosphorus into silicon. Finally, the phosphorus-doped silicon was treated with BOE solution to remove the SiO_2 coating layer on the surface. For comparison, the blank silicon wafer went through the same process except the reaction with PCl_3.

Surface Characterization. Infrared (IR) data were recorded in ambient air using Fourier transform infrared (FTIR) spectroscopy (Nicolet iN10 MX, Thermo Fisher Scientific). The transmission mode of liquid nitrogen-cooled MgCdTe detector has an angle of 90° away from the silicon surface. XPS was carried out using the Kratos AXIS UltraDLD spectrometer with a monochromatic AlKα source (1486.6 eV) in an analysis room with a pressure $<5 \times 10^{-9}$ Torr, a mixed-amplification mode analyzer, and a multi-channel detector at a takeoff angle of 45° from the sample surface. All binding energies were referenced to the C 1s signal (corrected to 285.0 eV). The XPS data results were processed using PeakFit software. AFM data were obtained through a Bio-fastScan atomic force microscope (model: Dimension Icon & FastScan Bio).

Sheet Resistance and Hall Test. A layer of 200 nm aluminum electrode was deposited on the surface of the sample by a thermal evaporation system. The sheet resistance was tested in a completely black metal box using the van der Pauw four-point method. The Keithley 2400 source instrument unit and custom-written Labview script were used to generate and collect current/voltage data. In the physical performance measurement system (PPMS, Quantum Design, USA), Hall measurement was performed on the DC resistivity sample holder pre-installed by wire bonding.

Secondary Ion Mass Spectrometry Test. The SIMS profiles of carbon and phosphorus were conducted at EAG laboratories in USA under a high vacuum condition of about 3×10^{11} Torr. Before depth carbon profiling, the samples were cleaned with oxygen plasma to remove possible carbon pollution in the environment.

■ ASSOCIATED CONTENT

Supporting Information

The Supporting Information is available free of charge at https://pubs.acs.org/doi/10.1021/acsaelm.1c00276.

XPS spectra of blank and doped samples, AFM images of doped samples, schematic diagram of the sheet resistance test, $I-V$ curves of samples, Hall effect measurements, and SIMS profile of phosphorus dopants and carbon impurities (PDF)

■ AUTHOR INFORMATION

Corresponding Author

Yaping Dan − *Key Laboratory for Thin Film and Microfabrication Technology of Ministry of Education, University of Michigan—Shanghai Jiao Tong University Joint Institute, Shanghai Jiao Tong University, 200240 Shanghai, China;* orcid.org/0000-0002-2983-7213; Email: yaping.dan@sjtu.edu.cn

Authors

Kai Li − *Key Laboratory for Thin Film and Microfabrication Technology of Ministry of Education, University of Michigan—Shanghai Jiao Tong University Joint Institute, Shanghai Jiao Tong University, 200240 Shanghai, China*

Jie-Yin Zhang − *National Laboratory for Condensed Matter Physics and Institute of Physics, Chinese Academy of Sciences, 100190 Beijing, China; CAS Center for Excellence in Topological Quantum Computation and School of Physics, University of Chinese Academy of Sciences, 100049 Beijing, China*

Shannan Chang − *Key Laboratory for Thin Film and Microfabrication Technology of Ministry of Education, University of Michigan—Shanghai Jiao Tong University Joint Institute, Shanghai Jiao Tong University, 200240 Shanghai, China*

Hao Wei − *Key Laboratory for Thin Film and Microfabrication Technology of Ministry of Education, University of Michigan—Shanghai Jiao Tong University Joint Institute, Shanghai Jiao Tong University, 200240 Shanghai, China;* orcid.org/0000-0001-5966-7174

Jian-Jun Zhang − *National Laboratory for Condensed Matter Physics and Institute of Physics, Chinese Academy of Sciences, 100190 Beijing, China; CAS Center for Excellence in Topological Quantum Computation and School of Physics, University of Chinese Academy of Sciences, 100049 Beijing, China*

Complete contact information is available at: https://pubs.acs.org/10.1021/acsaelm.1c00276

Notes

The authors declare no competing financial interest.

■ ACKNOWLEDGMENTS

This work was financially supported by the special-key project of Innovation Program of Shanghai Municipal Education Commission (2019-07-00-02-E00075) and National Natural Science Foundation of China (NSFC, 92065103). The devices were fabricated at the Center for Advanced Electronic Materials and Devices (AEMD), and Hall measurements were conducted at the Instrumental Analysis Center (IAC), Shanghai Jiao Tong University.

■ REFERENCES

(1) Ho, J. C.; Yerushalmi, R.; Jacobson, Z. A.; Fan, Z.; Alley, R. L.; Javey, A. Controlled nanoscale doping of semiconductors via molecular monolayers. *Nat. Mater.* **2008**, *7*, 62−67.

(2) Wang, D.; Sheriff, B. A.; Heath, J. R. Silicon p-FETs from ultrahigh density nanowire arrays. *Nano Lett.* **2006**, *6*, 1096−1100.

(3) Young, K. K. Short-Channel Effect in Fully Depleted Soi Mosfets. *IEEE Trans. Electron. Dev.* **1989**, *36*, 399−402.

(4) Chuang, S.-S.; Cho, T.-C.; Sung, P.-J.; Kao, K.-H.; Chen, H. J. H.; Lee, Y.-J.; Current, M. I.; Tseng, T.-Y. Ultra-Shallow Junction Formation by Monolayer Doping Process in Single Crystalline Si and Ge for Future CMOS Devices. *ECS J. Solid State Sci. Technol.* **2017**, *6*, P350−P355.
(5) Ho, J. C.; Yerushalmi, R.; Smith, G.; Majhi, P.; Bennett, J.; Halim, J.; Faifer, V. N.; Javey, A. Wafer-Scale, Sub-5 nm Junction Formation by Monolayer Doping and Conventional Spike Annealing. *Nano Lett.* **2009**, *9*, 725−730.
(6) Jones, E. C.; Ishida, E. Shallow junction doping technologies for ULSI. *Mater. Sci. Eng., R* **1998**, *24*, 1−80.
(7) Xiong, S.; Bokor, J. A Simulation Study of Gate Line Edge Roughness Effects on Doping Profiles of Short-Channel MOSFET Devices. *IEEE Trans. Electron Devices* **2004**, *51*, 228−232.
(8) O'Connell, J.; Verni, G. A.; Gangnaik, A.; Shayesteh, M.; Long, B.; Georgiev, Y. M.; Petkov, N.; McGlacken, G. P.; Morris, M. A.; Duffy, R.; Holmes, J. D. Organo-arsenic Molecular Layers on Silicon for High-Density Doping. *ACS Appl. Mater. Interfaces* **2015**, *7*, 15514−15521.
(9) Wu, H.; Guan, B.; Sun, Y.; Zhu, Y.; Dan, Y. Controlled doping by self-assembled dendrimer-like macromolecules. *Sci. Rep.* **2017**, *7*, 41299.
(10) Voorthuijzen, W. P.; Yilmaz, M. D.; Naber, W. J. M.; Huskens, J.; van der Wiel, W. G. Local Doping of Silicon Using Nanoimprint Lithography and Molecular Monolayers. *Adv. Mater.* **2011**, *23*, 1346−1350.
(11) Taheri, P.; Fahad, H. M.; Tosun, M.; Hettick, M.; Kiriya, D.; Chen, K.; Javey, A. Nanoscale Junction Formation by Gas-Phase Monolayer Doping. *ACS Appl. Mater. Interfaces* **2017**, *9*, 20648−20655.
(12) Gao, X.; Guan, B.; Mesli, A.; Chen, K.; Dan, Y. Deep level transient spectroscopic investigation of phosphorus-doped silicon by self-assembled molecular monolayers. *Nat. Commun.* **2018**, *9*, 118.
(13) Wu, H.; Li, K.; Gao, X.; Dan, Y. Phosphorus ionization in silicon doped by self-assembled macromolecular monolayers. *AIP Adv.* **2017**, *7*, 105310.
(14) Gao, X.; Kolevatov, I.; Chen, K.; Guan, B.; Mesli, A.; Monakhov, E.; Dan, Y. Full Activation of Boron in Silicon Doped by Self-Assembled Molecular Monolayers. *ACS Appl. Electron. Mater.* **2020**, *2*, 268−274.
(15) Longo, R. C.; Cho, K.; Hohmann, S.; Thissen, P. Mechanism of Phosphorus Transport Through Silicon Oxide During Phosphonic Acid Monolayer Doping. *J. Phys. Chem. C* **2018**, *122*, 10088−10095.
(16) Longo, R. C.; Cho, K.; Schmidt, W. G.; Chabal, Y. J.; Thissen, P. Monolayer Doping via Phosphonic Acid Grafting on Silicon: Microscopic Insight from Infrared Spectroscopy and Density Functional Theory Calculations. *Adv. Funct. Mater.* **2013**, *23*, 3471−3477.
(17) Zhi, K.; Zhang, C.; Wei, H.; Wen, H.; Dan, Y. Thermal pyrolysis investigation of self-assembled molecular monolayer for defect-free doping in silicon. *Chem. Phys.* **2020**, *531*, 110658.
(18) Gao, X.; Guan, B.; Mesli, A.; Chen, K.; Sun, L.; Dan, Y. Toward Defect-Free Doping by Self-Assembled Molecular Monolayers: The Evolution of Interstitial Carbon-Related Defects in Phosphorus-Doped Silicon. *ACS Omega* **2019**, *4*, 3539−3545.
(19) van Druenen, M.; Collins, G.; Glynn, C.; O'Dwyer, C.; Holmes, J. D. Functionalization of SiO2 Surfaces for Si Monolayer Doping with Minimal Carbon Contamination. *ACS Appl. Mater. Interfaces* **2018**, *10*, 2191−2201.
(20) Ye, L.; González-Campo, A.; Núñez, R.; de Jong, M. P.; Kudernac, T.; van der Wiel, W. G.; Huskens, J. Boosting the Boron Dopant Level in Monolayer Doping by Carboranes. *ACS Appl. Mater. Interfaces* **2015**, *7*, 27357−27361.
(21) Juang, A.; Scherman, O. A.; Grubbs, R. H.; Lewis, N. S. Formation of covalently attached polymer overlayers on Si(111) surfaces using ring-opening metathesis polymerization methods. *Langmuir* **2001**, *17*, 1321−1323.
(22) Lin, G.-R.; Lin, C.-J.; Lin, C.-K. Defect-enhanced photoconductive response of silicon-implanted borosilicate glass. *Appl. Phys. Lett.* **2004**, *85*, 935−937.

https://doi.org/10.1021/acsaelm.1c00276
ACS Appl. Electron. Mater. 2021, 3, 3346−3351